Eur. Phys. J. A **7**, 483–490 (2000)

THE EUROPEAN PHYSICAL JOURNAL A

Microscopic analysis of the breathing mode in ^{40}Ca and ^{58}Ni

S. Kamerdzhiev[1,2], J. Speth[1], G. Tertychny[1,2]

[1] Institut für Kernphysik, Forschungszentrum Jülich, 52425 Jülich, Germany
[2] Institute of Physics and Power Engineering, 249020 Obninsk, Russia

Received: 23 December 1999 / Revised version: 28 February 2000
Communicated by P. Schuck

Abstract. Recent experimental studies of the giant electric resonance region in ^{58}Ni and ^{40}Ca with inelastically scattered α-particles of energy $E_\alpha = 240$ MeV are analyzed within a microscopic nuclear structure model.

The model includes the continuum RPA and more complex 1p1h⊗phonon configurations. By superimposing the contributions of different multipoles up to L = 4 we obtain good agreement with the newest (reanalyzed) data for the isoscalar monopole strength and for the total (α, α') cross section in ^{58}Ni. Agreement with experiment for the isoscalar monopole resonance in ^{40}Ca is obtained too. We emphasize the necessity of using microscopic transition densities and discuss consequences for the analyses of such experiments in light and medium mass nuclei. It is shown that the gross structure of the isoscalar monopole resonance in ^{40}Ca is caused by the 1p1h⊗phonon configurations.

PACS. 24.30.Cz Giant resonances – 25.55.Ci Elastic and inelastic scattering – 27.40.+z $39 \leq A \leq 58$

1 Introduction

The isoscalar electric monopole (IS E0) giant resonance in nuclei is a unique source of information on the compressibility and equation of state of nuclei. The extrapolation to nuclear matter and neutron stars requires that the energy of the resonance has to be known over a wide range of the mass number A. However, until very recently, there were several open questions connected with the IS E0 resonance in nuclei with A<90 [1]. Here, the monopole strength is no longer concentrated in one narrow peak, and, in some cases, also the magnitude of the detected strength was much smaller than the energy-weighted-sum-rule (EWSR) limit. An important example in this connection is ^{58}Ni, where originally only 32% of the EWSR was observed with inelastically scattered α-particles [2]. These authors used the standard data-analysis procedures with phenomenological transition densities ρ^L_{tr} which were the same for different excitation energies. For comparison, the same type of experiment in ^{40}Ca and a similar data-analysis by the same authors showed (92 ± 15)% of the EWSR [3]. Such uncertainties may have serious consequences for the nuclear matter compressibility and its applications in astrophysics. An improved analysis of the ^{58}Ni data [2] by Satchler and Khoa [4], based upon the most consistent folding models for the transition potentials, gave about 50% of the EWSR.

Our analysis of the same experimental data [5], where microscopic transition densities have been used, gave 71.4% of the IS E0 EWSR in the (12.0-25.0) MeV interval. The microscopic model used took into account all three known mechanisms of giant resonance damping, namely the RPA or Landau damping, the spreading width caused by more complex 1p1h⊗phonon configurations and the escape width due to the inclusion of the single-particle continuum. The known parameters of the Landau-Migdal effective interaction have been used in our approach. Because of the energy-dependence of the microscopic transition densities, the energy interval considered was divided into 5 MeV bins for which the calculations were performed separately. The results of the calculations allowed the assumption [5] that a part of the IS E0 strength in ^{58}Ni might be hidden in the experimental background.

In the meantime the energy range of the original experiment in ^{58}Ni (12 - 25) MeV has been extended [6] to (12 - 35) MeV. From a preliminary analysis the authors concluded that between 75 -100% of the EWSR has possibly been detected, see also [7]. Very recently, these data have been finally analyzed in [8]. Here the authors present results from the (12.0-31.1) MeV excitation region. Thus we are now able to compare their results with our previous calculations in more detail and we report in our present work also on an extended analysis of the new experimental data. Compared with the original analysis by Youngblood et al. in [2], two new ingredients were included by the same authors in their new work [8]: 1)a nuclear reaction description was used following the methods of [4], 2)the giant resonance peak obtained after subtraction of the continuum (see the experimental curve in Fig. 7 be-

low) was divided into 15 energy intervals from 1 to 3 MeV each of which was analyzed separately.

It is a general problem in A<90 nuclei that the isoscalar monopole resonance is very broad and no longer concentrated in one single peak. In lighter nuclei, the role of the surface becomes more important than in heavy nuclei, and in addition the (α,α') reaction is very sensitive to the nuclear surface. Moreover, for light and medium mass nuclei the single -particle continuum becomes very important. For instance, we showed in [9] that the contribution of the continuum to the calculated total width of the E1 resonance for ^{40}Ca and ^{48}Ca was 14% and 28%, respectively, but only 7% for ^{208}Pb. All of this has to be considered if theoretical models for giant resonances in lighter nuclei are developed. The conventional approach to collective states, the random phase approximation (RPA), has to be extended by the inclusion of surface modes and the single-particle continuum, at least on the RPA level. Such a microscopic nuclear structure model was developed by us in the past years [9–11]. It considers, in addition to the continuum RPA, also the low-lying collective states in a consistent way.

In the following we report on the analysis of the (α,α') experiments in ^{58}Ni and ^{40}Ca, where the isoscalar giant resonance region has been investigated. Within our microscopic model, we calculate the strength distributions of the isovector E1 and isoscalar E0 - E4 resonances and the corresponding transition densities. From these transition densities we obtain, in the standard way, (α,α') cross sections which we compare with the experimentally known data in ^{40}Ca in the observed (8.0-29.0) MeV interval [3] (only for the IS E0 resonance), and for the isotope ^{58}Ni in three energy regions: (12 - 25) MeV [2], (12.0-31.1) MeV [8] and also (12 - 35) MeV [6,7]. Some preliminary results of our calculations have been presented in [5].

2 Theory

The nuclear structure part, i.e. the transition quantities ρ^L_{tr}, which are the main ingredients of a microscopic approach for (α,α') cross sections, are calculated within our approach which is described in detail in [9–11]. Here the basic equations of our calculations will be given.

2.1 Nuclear structure: density matrix and strength function

The basic equation for the density matrix is formulated in coordinate space. In fact, it is the change of the density matrix in an external field V^0 with the energy ω:

$$\rho(\mathbf{r},\omega) = -\int A(\mathbf{r},\mathbf{r}',\omega) e_q V^0(\mathbf{r}') d^3r' - \int A(\mathbf{r},\mathbf{r_1},\omega) F(\mathbf{r_1},\mathbf{r_2}) \rho(\mathbf{r_2},\omega) d^3r_1 d^3r_2. \quad (1)$$

Here e_q and F are the local quasiparticle charge and the effective interaction, respectively. As discussed in [9–11], they are taken from the theory of finite Fermi-systems, *e.g.* the interaction is given by

$$F(\mathbf{r},\mathbf{r}') = C_0[f(r) + f'(r)\boldsymbol{\tau_1}\boldsymbol{\tau_2} + (g + g'\boldsymbol{\tau_1}\boldsymbol{\tau_2})\boldsymbol{\sigma_1}\boldsymbol{\sigma_2}]\delta(\mathbf{r}-\mathbf{r}'), \quad (2)$$
$$f(r) = f_{ex} + (f_{in} - f_{ex})\rho_0(r)/\rho_0(0),$$

where $\rho_0(r)$ is the nuclear density in the ground state. For the latter we use the calculated nuclear density in the ground state

$$\rho_0(r) = \sum_{\epsilon_i \le \epsilon_F} \frac{1}{4\pi}(2j_i+1)R_i^2(r), \quad (3)$$

where $R_i(r)$ are radial single-particle wave functions.

In (1), all of the difference from the usual RPA is contained in our generalized propagator A. It consists of two parts: the RPA-like part and the part which contains much more complicated physics caused by 1p1h⊗phonon configurations including ground state correlations induced by these complex configurations. The expression for the propagator A is given by

$$A(\mathbf{r},\mathbf{r}',\omega) = \tilde{A}^{RPA}_{cont}(\mathbf{r},\mathbf{r}',\omega) + \sum_{1234}(A_{1234}(\omega) - \tilde{A}^{RPA}_{1234}(\omega)\delta_{13}\delta_{24})\tilde{\varphi}^*_1(\mathbf{r})\tilde{\varphi}_2(\mathbf{r})\tilde{\varphi}_3(\mathbf{r}')\tilde{\varphi}^*_4(\mathbf{r}'), \quad (4)$$

where $\tilde{A}^{RPA}_{cont}$ is the "refined" RPA propagator in which the single-particle continuum is taken into account exactly. The summation in (4) is performed over two shells above and all shells below the Fermi level. The expression for the propagator A_{1234} was obtained in the "refined" single-particle basis $(\tilde{\varphi}_\lambda, \tilde{\epsilon}_\lambda)$ and discussed in detail in [10]. It has a rather cumbersome form which we do not write down here. (We have used a refinement procedure [9–11] for the phenomenological single-particle basis to avoid double counting of the phonons containing in the 1p1h⊗phonon configurations under consideration).

Thus, our microscopic approach takes into account the single-particle continuum, RPA configurations and more complex 1p1h⊗phonon ones, as well as ground state correlations induced by these complex configurations. We have demonstrated in [11] that these additional configurations are essential for a quantitative description of giant resonances in ^{40}Ca, ^{48}Ca. and ^{56}Ni. Because only in the RPA part of the propagator the single particle continuum is taken into account completely, the continuum is somewhat underestimated in our approach.

The excitation energies are determined by solving system of homogeneous equations which are obtained from (1). The squared amplitudes of the transition between the ground and excited states are given by the residues at the excitation energies of the polarizability operator,

$$\Pi(\omega) = \int d^3r [e_q V^0(\mathbf{r})]^* \rho(\mathbf{r},\omega). \quad (5)$$

We did not use, however, this approach directly and calculated the strength function which gives the energy

distribution of the excitation strength under consideration:

$$S(E,\eta) = \frac{dB(EL)}{dE} = -\frac{1}{\pi} Im\Pi(E+\imath\eta), \qquad (6)$$

where η is a smearing parameter. Using this parameter we take into account phenomenologically those complex configurations which are not explicitly treated, and simulate a finite experimental resolution. Then the EWSR, summed in the energy interval $[E_1, E_2]$,

$$\Sigma_L = \sum_{[E_1,E_2]} E_i B_i(EL) \uparrow \qquad (7)$$

can easily be obtained from (6).

In principle, our model is applicable only to closed shell nuclei, e.g. to ^{56}Ni. However, ^{58}Ni differs only little from ^{56}Ni. From our point of view, the main difference is the addition of the 2^+ and 4^+ (two-nucleon) excitations which are energetically below the collective "particle-hole" excitations. The latter are practically identical for ^{56}Ni and ^{58}Ni. In our 1p1h$\otimes$phonon configurations for ^{58}Ni, we consider these low-lying states in addition to the low-lying collective 2^+, 3^-, 5^-, 4^+ and 6^+ phonons which are already taken into account in our previous investigations of ^{56}Ni [11,12].

2.2 Cross sections

The transition densities ρ^L_{tr}, which are used in phenomenological and microscopic models, are simply connected with our density matrix $\rho_L(r, E+\imath\eta)$ determined in (1):

$$\rho^L_{tr}(r,\Delta E) = \frac{1}{\pi\sqrt{\Sigma B(EL)}} Im \int_{E_{min}}^{E_{max}} dE \rho_L(r, E+\imath\eta), \quad (8)$$

where $\Sigma B(EL)$ is the $B(EL)$ value summed over the interval ΔE.

The calculation of the cross sections was carried out with the modified code DWUCK4. The multipole transition potentials were constructed by single-folding the complex density-dependent Gaussian effective α-nucleon interaction [4] with our microscopic ρ^L_{tr} for ^{58}Ni under the prescription given in [13]. The strength and range of the real and imaginary parts of the effective interaction have been adjusted to the experimental cross sections of the low-lying 2^+ and 3^- collective states [2]. The parameters of the optical model potential were taken from [14]. As in the analysis of [2,8], contributions of the IS and IV E1 and IS E0, E2, E3, E4 resonances, which were calculated within our approach in the region under consideration, have been taken into account.

In the present analysis of the (α,α') cross sections the following procedure has been used. The theoretical transition densities for each of the 6 EL resonances were analyzed over 5 MeV energy intervals for ^{58}Ni and these densities were used as input into the DWUCK4 code. For every energy interval, the DWBA cross sections $d\sigma_L(\overline{E}_L,\theta)/d\Omega$ have been calculated. Then the inelastic α spectrum has been obtained from the expression

$$\frac{d^2\sigma}{d\Omega dE}(E,\theta) = \sum_L \frac{2}{\pi\Gamma_L} \frac{(\Gamma_L/2)^2}{(E-\overline{E}_L)^2+(\Gamma_L/2)^2} \frac{d\sigma_L}{d\Omega}(\overline{E}_L,\theta). \qquad (9)$$

Here the summation runs over the 6 multipolarities considered and the parameters $\overline{E}_L$ and Γ_L have been obtained from a Lorentz fit to the calculated strength function $S_L(E)$ (6). For ^{40}Ca, we have used 2 MeV intervals, and the above-mentioned procedure has been performed only for the IS E0 resonance.

In our calculations we used a standard Woods-Saxon single-particle basis. The residual Landau-Migdal interaction with known parameters has been used. The latter allows to calculate and predict properties of unknown, e.g. unstable nuclei, because the parameters of this interaction are known and should be suitable for all nuclei except for light ones. The values and the detailed choice of these parameters, as well as the characteristics of the phonons, which were calculated microscopically, may be found in [10–12,15]. The present model with the present parameters was successfully applied to the analysis of $(e,e'x)$ data in ^{40}Ca [16,15].

In all our calculations, the smearing parameter η = 500 keV has been used.

3 Results

3.1 Microscopic transition densities

In the previous analysis of ^{40}Ca, ^{48}Ca and ^{56}Ni [11], we found that the radial form of the transition density varies over the energy range considered and it depends also to some extend on the length of the energy bins choosen. In this respect, the microscopic ρ_{tr}'s are very different from the phenomenological ones used in conventional analyses, where they are considered energy independent over the whole energy interval.

In Fig. 1 we compare the phenomenological transition densities for the IS E0 resonance in ^{40}Ca with the theoretical transition densities obtained for two 2 MeV intervals in the main part of the resonance. We see a noticeable difference, for the two intervals, both among the theoretical densities and between the theoretical and phenomenological densities.The behaviour of the microscopic and phenomenological densities near the nuclear surface, to which the (α,α') cross sections are most sensitive, is very different in the two intervals considered. Inside the nucleus, the behaviour of the transition densities differs also strongly for the two intervals. E.g., for the (17-19) MeV interval, the neutron microscopic density has three nodes whereas the IS E0 phenomenological transition density has always only one node.

Differential cross sections calculated with the transition densities of Fig. 1 are shown in Fig. 2. The values of the ratio M_n/M_p of the nuclear transition momenta, which is adopted to be equal to 1 for ^{40}Ca in the phenomenological approach, are also given in Figs. 1 and 2.

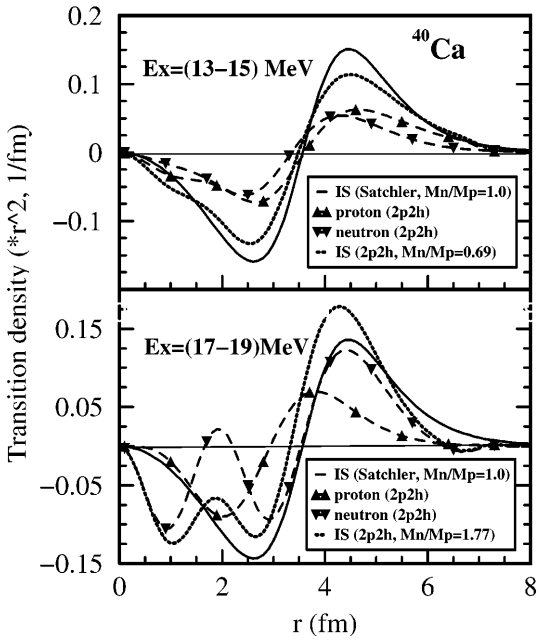

Fig. 1. The microscopic (dotted line) and phenomenological (solid line) IS E0 transition densities in ^{40}Ca, calculated for two different energy intervals of 2 MeV each. Results for proton and neutron microscopic transition densities are also given (denoted by triangles). The values of the corresponding ratio M_n/M_p of the nuclear transition momenta are given in the legend

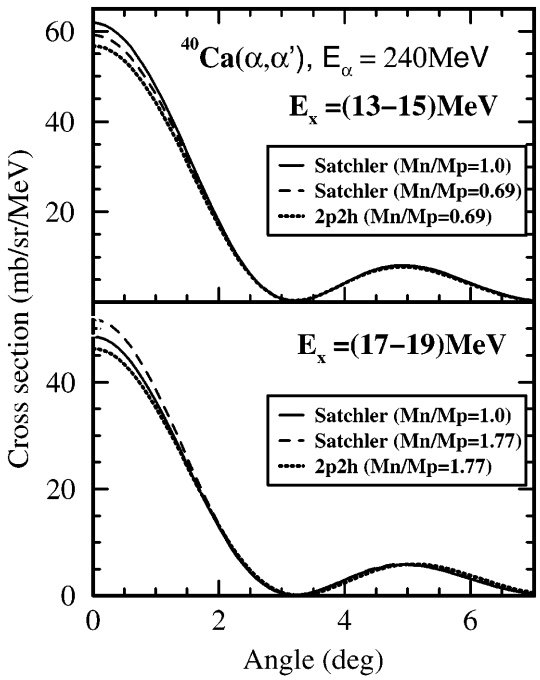

Fig. 2. Angular distributions for the IS E0 resonance in the same intervals as in Fig. 1, calculated with the phenomenological and microscopic transition densities. For comparison, the results (dashed line) with the phenomenological transition density, obtained with the microscopic value of the ratio M_n/M_p of the nuclear transition momenta, are also shown

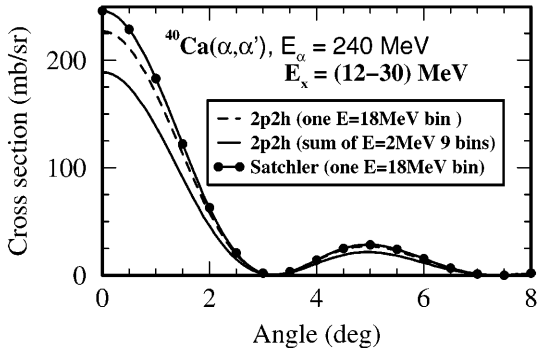

Fig. 3. Angular distributions for the IS E0 resonance in ^{40}Ca in the (12 - 30) MeV interval, calculated under two methods: the division the interval into 9 bins of 2 MeV each (solid line) and the interpretation of the (12 - 30) MeV interval as one bin (dashed line), respectively. For comparison, the results obtained with the phenomenological transition density are also given (solid curve with dots)

In the microscopic approach, there is a noticeable difference of the M_n/M_p ratio both with respect to themselves for the two intervals and between the phenomenological and microscopic densities. The cross sections calculated with phenomenological densities taken at microscopic values of M_n/M_p are also shown. The various cross sections differ most around zero degree where our theoretical cross sections are smaller by 5-8% compared to the phenomenological analysis.

In order to demonstrate the role of the size of the energy interval, we compare two theoretical ^{40}Ca(α, α') differential cross sections for the IS E0 giant resonance in Fig. 3. The dashed line is derived from a transition density averaged over the whole energy range (12 - 30) MeV. The full line corresponds to the differential cross sections which were obtained by the discussed procedure performed for the 2 MeV bin and summed over the same energy range (12 - 30) MeV. As we can see, around zero degree the two cross sections calculated with microscopic densities differ by nearly 25%. The difference between Satchler's results and our 2 MeV differential cross section is even larger.

In addition to the energy-dependence, there are further important differences between microscopic and phenomenological transition densities: (i) In the microscopic approach, the simple relationships for the proton and neutron components of the nuclear transition momenta (as discussed above) and transition densities such as the ones with the ratio Z/N, do not exist. This fact results in a specific energy dependence of the Coulomb-nuclear interference in total transition potentials, which may even change a destructive interference into a constructive one. (ii) Also the multipole decompositions of the cross sections are very different in the phenomenological approach compared to the microscopic one. In the first case one tries to extract the corresponding multipole composition by fitting to various total and differential experimental cross sections. In the microscopic approach, these multipole decompositions are determined within the theoretical model with known parameters. Indeed, our microscopic results deviate ap-

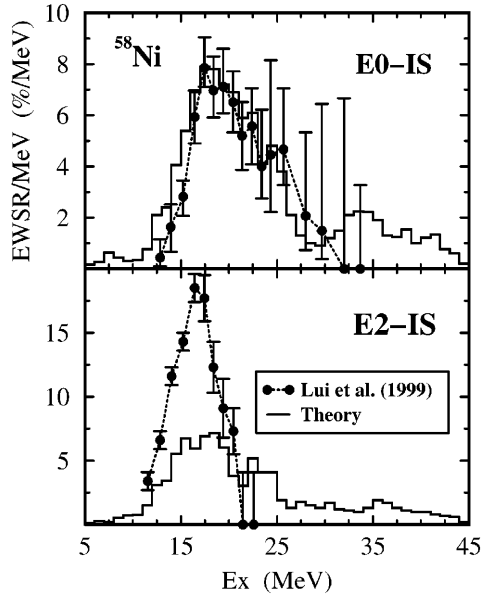

Fig. 4. Distribution of the IS E0 and E2 strengths in ^{58}Ni. The experimental data are taken from [8]

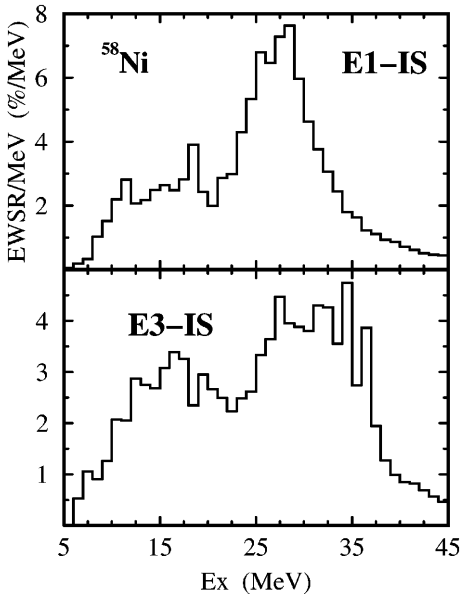

Fig. 5. Distribution of the IS E1 and E3 strengths in ^{58}Ni as calculated within our theoretical model

preciably from the ones derived from phenomenological approaches.

3.2 ^{58}Ni results

In Fig. 4 we compare our microscopic calculations with the newest experimental results given in [8] for the IS E0 and E2 strength distributions. For the observed (12.0-31.1) MeV interval, we obtained a value of the mean energy of the IS E0 resonance equal to 19.9 MeV (defined as m_1/m_0) and find 81.5% of the EWSR. The experimental data are $(20.30^{+1.69}_{-0.14})$ MeV and (74^{+20}_{-6})%, respectively. For the "old" (12.0-25.0) MeV interval, the new phenomenological analysis finds (58±6)% of the EWSR [8] which is now much closer to the microscopic value of 71.4% [5] obtained for the same interval. Therefore, both analyses give now very similar results.

However, as one can see from the lower part of Fig. 4, for the IS E2 strength the two approaches come still to quite different conclusions. Our E2 resonance mean energy value and the depletion of the IS E2 EWSR defined in the (10.0-20.0) energy interval are 19.1 MeV and 47%, while the phenomenological analysis gives 16.1 MeV and (115±15)%, respectively. There is also a disagreement for the IS E1 and E3 strengths. Our results are represented in Fig. 5 (see also the discussion at the end of this subsection).

The numerical role of the complex configurations 1p1h⊗phonon in^{58}Ni considered in our approach can be seen from the results for the neighbouring isotope ^{56}Ni obtained by us earlier in [11]. These calculations were performed within the same numerical scheme as that for ^{58}Ni and, therefore, should be similar to the results for ^{58}Ni. As can be seen in Fig. 2 from [11], the strength distribution obtained with complex configurations appears to be much more noticeably structured vs.that obtained without complex configurations, i.e. for the RPA case. (Note that the E0-EM strength is similar enough to that of E0-IS up to about 28 MeV, see Fig. 3, ibid). A particulary high difference, more than two-fold, is found for the main peak at about 17 MeV.

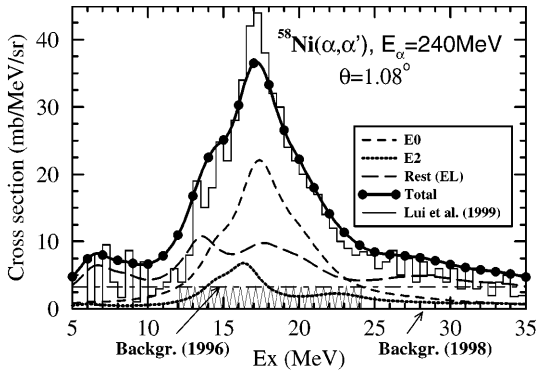

Fig. 6. Cross sections of ^{58}Ni(α, α') at E_α = 240 MeV and $\theta = 1.08°$. The experimental data (hystogram) were taken from [8] where an instrumental background has been substracted. The solid curve with dots gives the calculated total (summed) cross sections, the dashed line ("Rest(EL)") corresponds to the sum of the IS and IV E1, and IS E3 and E4 multipoles. The shaded area shows an additional IS E0 strength which has been substracted in the previous experiments as background [2]. This area corresponds to 22% of the IS E0 EWSR

In Figs. 6 and 7 we compare the same experimental data in a slightly different way with our theoretical results, where we obtain in both cases good agreement between our theory and the data for the total cross sections.

In Fig. 6, we show the role of background and the contribution of the various giant resonances to the total cross section. We compare our theoretical results (full line with

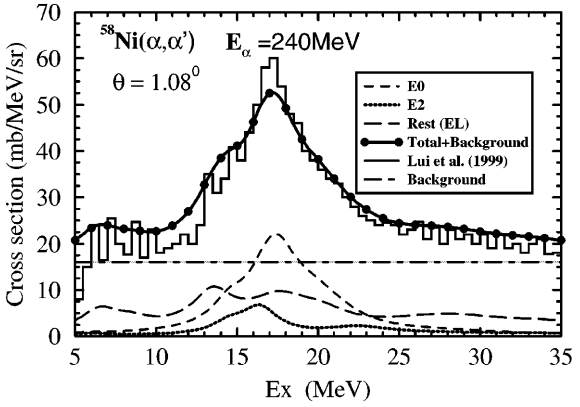

Fig. 7. Cross sections of ^{58}Ni(α,α') at E$_\alpha$ = 240 MeV and $\theta = 1.08°$. The experimental data (hystogram) including the instrumental background are taken from [8]. The solid curve with dots gives the calculated total (summed) cross sections. In the lower part of the picture the components of the total cross sections are shown without the background. In particular, the dashed line gives the IS E0 contribution

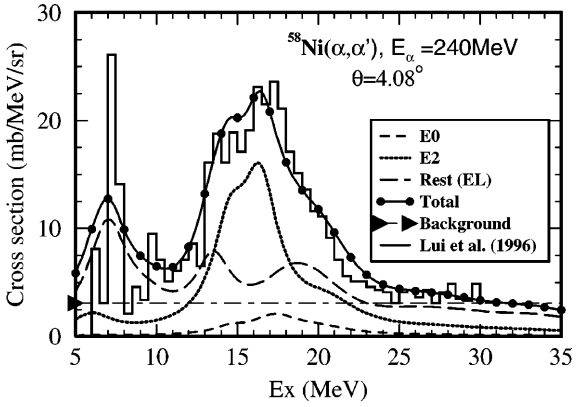

Fig. 8. Same as in Fig. 7 but for $\theta = 4.08°$. The experimental data were produced in the present article using the results of [2], see text

dots) with the experimental cross section at $\theta = 1.08°$ (hystogram) of [6,8]. These data were obtained by us by subtracting an instrumental background from the original experimental spectrum. The theoretical cross section is the sum of 6 different multipoles, from which we only show E0 and E2. The straight line in the lower part of the figure denoted by "Backgr.(1996)" corresponds to the previous analysis of [2], where the considered energy interval (12 - 25) MeV was smaller. In the original analysis, with phenomenological transition densities, only 32% of the IS E0 EWSR limit was found. With the improved, but still conventional analysis, the authors of [4] obtained about 50%.

In Fig. 6, we also compare the (12 -25) Mev interval and the previous background subtraction with the new extended interval and the experimental data where a different background has been substracted. Here we come to the following conclusion: In our analysis the total IS E0 resonance cross section in the (12 - 25) MeV energy range corresponds to 71.4% of EWSR and is equal to 138.3 mb/sr. The area under the old background line in this region, which is included in our 71.4% of EWSR, corresponds to 22% of the IS E0 EWSR limit or 42.6 mb/sr. This strength had been substracted as a part of the background in [2] and correspondingly was not included in the analysis of [4].

If we extend the analysis to the larger (12 - 35) MeV interval, our theoretical model predicts 89.6% of the IS E0 EWSR limit.

In Fig. 8 we compare our theoretical cross sections with the data at $\theta = 4.08°$. We reconstructed the experimental cross section from Fig. 4 and Fig. 1 of [2]. Good agreement between the theory and previous experiment [2] is obtained. We also see that, at this angle, the IS E2 resonance and higher multipoles contribute most to the cross section, whereas the monopole contribution is small.

Thus, one can conclude that the new experimental data for the IS E0 resonance in ^{58}Ni are in good agreement with the microscopic calculations which do not contain any fitting parameters. The values of integral characteristics correspond now to the known experimental systematics. In particular, as was noted in [8], the E0 strength located in ^{58}Ni is consistent with recent results for ^{40}Ca, ^{28}Si and ^{24}Mg. All these results allow for the hope that the problem of the IS E0 resonance in nuclei with A<90 [1,7] has been solved.

However, the disagreement between our microscopic results and the phenomenological analysis [8] for the IS E2 resonance only confirms our earlier conclusion [5] about the necessity of using microscopic transition densities in the experimental analysis. The same is true for the IS E1 resonance, where the two approaches come also to very different conclusions. The authors [8] obtained only 41% of the IS E1 EWSR and this strength was spread "more or less" uniformly from 12 MeV to 35 MeV. Our distribution of this strength is shown in Fig. 5. One can see that there is no uniform distribution but we have a resonance structure. We obtained 89% of the IS E1 EWSR and a value of 25.0 MeV for the mean energy in the interval under consideration. These figures are consistent with the results of [17] for other nuclei. Our E3 IS strength is more uniformly distributed.

3.3 ^{40}Ca results

Our improved calculations of the IS E0 resonance in ^{40}Ca, presented in [11], show that it has a more compact form than in our earlier calculations [18]. But it remains strongly structured and spread-out over a large energy interval: 65% of the EWSR is in the (11-23) MeV interval and 106.7% is in the (5.0-45.0) MeV interval [10]. Thus, it is important that the large energy interval (8.0-29.0) MeV was studied in [3] and, in fact, most of the IS E0 strength was found in their analysis.

In Fig. 9 our theoretical distributions of the IS E0 and E2 strengths in ^{40}Ca are shown. As compared with the

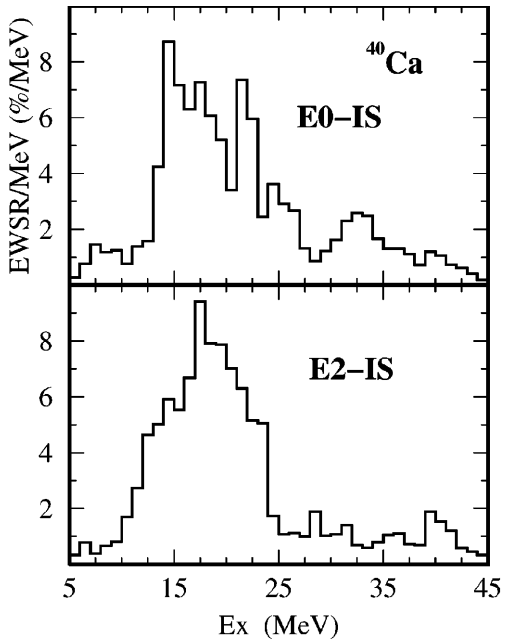

Fig. 9. Distribution of the IS E0 and E2 strengths in ^{40}Ca (theory)

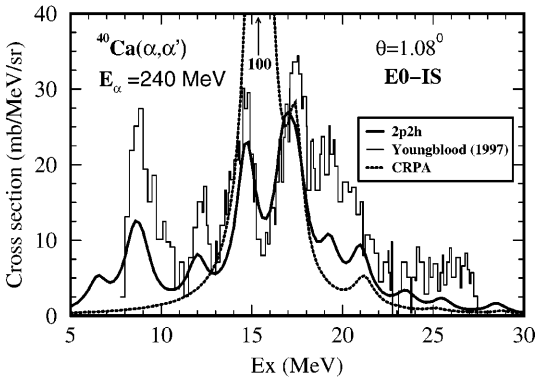

Fig. 10. The 0° cross section for the IS E0 strength in ^{40}Ca(α, α') at E_α = 240 MeV, calculated with (dashed line) and without (dotted line) taking into account complex 1p1h⊗phonon configurations. The experimental data (hystogram) are taken from [3]. One can see that the gross structure of the IS E0 resonance is caused by complex 1p1h⊗phonon configurations

corresponding results of the analysis of [3], which were obtained from the difference between spectra taken at $\theta = 1.1°$ and $\theta = 2.4°$ (see Fig. 6 of [3]), a reasonable agreement for the central part (10 - 23) MeV of the IS E0 resonance is obtained. The percentages of the IS E0 EWSR in the four observed intervals (7.5-12.5) MeV, (12.5-22.5) MeV, (22.5-28.8) MeV and (7.5-28.8) MeV are as follows: 6.0(7.6±0.2)%, 60.0(50.0±1.4)%, 16.0(34.7±1.7)% and 81.6(92±2)%,respectively (in brackets, we have listed the results of [3] with only statistical errors). The final result of the analysis of [3] for the IS E0 EWSR between 8<E$_x$<29 MeV is (92±15)% which agrees with our value of 81.6%. However, there is a noticeable disagreement in the low-lying and high-lying regions of the excitation spectrum.

In [3] the authors find (33±4)% of the IS E0 EWSR and (57±6)% of the IS E2 EWSR at a peak energy of (17.5±0.4) MeV. Our results for the IS E0 and E2 resonance mean energies, obtained (as m_1/m_0) from averaging over the observed (8.0 - 29.0) MeV interval, are 17.2 MeV and 17.1 MeV, respectively. It is impossible to compare the experimental IS E0 EWSR depletion value with our value of 81.6%, and one of the reasons is that the experimental value of (33±4)% does not contain the continuum, see [3]. However, for the IS E2 resonance, the difference between our value of 88.0%, obtained for the (8.0-29.0) MeV interval, and 57% of [3] is smaller which may indicate that there is less E2 strength in the experimental continuum.

A more distinct comparison with experiment is shown in Fig. 10 [3] for the double-differential cross section for ^{40}Ca. Our full calculations reproduce the experimental gross structure reasonably well, but, again, we have a difference at low and high energies. The general difference in the values of the theoretical and experimental cross sections may give a hint that other multipoles than IS E0 contribute to that cross section.

To understand better the role of complex configurations, we also show in Fig. 10 (α, α') cross sections obtained with the microscopic transition density calculated within the continuum RPA only, i.e. without inclusion of our complex 1p1h⊗phonon configurations. It can easily be seen that there is a big difference between two theoretical curves. We conclude that the gross structure of the IS E0 resonance in ^{40}Ca is caused by the complex 1p1h⊗phonon configurations. A similar conclusion for fine structure of the IS E2 resonance in ^{208}Pb was obtained in our calculations [19].

4 Conclusion

Using a microscopic nuclear structure model that takes into account the continuum RPA and 1p1h⊗phonon configurations, we were able to describe the newest (reanalysed) experimental data for ^{58}Ni(α, α') in the observed energy intervals [8] and to obtain a reasonable agreement with similar experimental data for the IS E0 resonance in ^{40}Ca [3]. The theoretical cross sections do not contain any parameters adjusted to the present experimental data. Bearing this in mind, the agreement between theory and experiment is overall very reasonable.

The method presented here is of general interest for the analysis of giant resonances in light and medium mass nuclei. We start with a nuclear structure model which allows for the calculation of width and distribution of giant multipole resonances. All the multipole contributions in a given energy range are considered and summed up. Due to the superposition of very different multipole resonances, we obtain cross sections which show peaks on a flat background. However, this flat background is not only an instrumental one, but contains an appreciable amount of the resonance multipole strength. This, in fact, has been shown in the newest analysis of the ^{58}Ni(α, α') experimen-

tal data [8] which is now in agreement with our earlier conclusion [5]. At present, the IS E0 strength in ^{58}Ni is consistent with recent experimental results for light nuclei including ^{40}Ca. All of this allows us to hope that the problem of the IS E0 strength in nuclei with A<90 has now been solved.

Although the comparison of microscopic calculations with the experiment, where phenomenological transition densities have been used, shows a good overall agreement, we would like to emphasize that it is necessary to use microscopic transition densities in the experimental analysis. This is especially important for the A<90 nuclei where the giant resonances are strongly structured and spread out over a large energy region. On one hand, we obtained IS E2, E1 and E3 strengths in ^{58}Ni, which are in better agreement with results for other nuclei than with the ones extracted from analysis for the ^{58}Ni case [8] with phenomenological transition densities. On the other hand, the use of microscopic transition densities makes it possible to single out important and interesting physical effects, like the role of complex configurations (as was shown in Fig. 10) or ground state correlations induced by these configurations, or, maybe, more delicate effects which may arise in experiments with a better resolution and efficiency of the detectors.

We thank D.H. Youngblood and Y.-W. Lui for useful discussions, the permission to publish their experimental data and for sending us their article [8]. We thank A. Wirzba for a careful reading of manuscript. The work was partly supported by the German-Russian Exchange Program, Deutsche Forschungsgemeindschaft (contract 436RUS17/88/96) and Russian Fund for Fundamental Research, grant No.96-02-17250.

References

1. A. van der Woude, in *Electric and Magnetic Giant Resonances in Nuclei*, edited by J. Speth (World Scientific, Singapore, 1991), p. 99
2. D.H. Youngblood, H.L. Clark, and Y.-W. Lui, Phys. Rev. Lett. **76**, 1426 (1996)
3. D.H. Youngblood, Y.-W. Lui, and H.L. Clark, Phys. Rev. C **55**, 2811 (1997)
4. G.R. Satchler and Dao T. Khoa, Phys. Rev. C **55**, 285 (1997)
5. S. Kamerdzhiev, J. Speth, and G. Tertychny, IKP Annual Report 1996, p.201; in Proceedings of the Intern. Conference on Nuclear Structure and Related Topics, edited by S.N. Ershov, R.V. Jolos and V.V. Voronov, Dubna, September 1997, p. 347; in Proceedings of the Workshop on the Structure of Mesons, Baryons and Nuclei, Cracow, May 1998, edited by S. Drożdż and S. Krewald, Acta Phys. Pol. B **29**, 2231 (1998)
6. Y.-W. Lui, D.H. Youngblood, and H.L. Clark, Contribution to the Topical Conference on Giant Resonances, Italy, Varenna, May 1998
7. A.van der Woude, Nucl. Phys. **A649**, 97c (1999)
8. Y.-W.Lui, H.L. Clark and D.H. Youngblood, Preprint, submitted to Phys. Rev. C
9. S. Kamerdzhiev, J. Speth, G. Tertychny, and V. Tselyaev, Nucl. Phys. **A555**, 90 (1993)
10. S. Kamerdzhiev, G. Tertychny, and V. Tselyaev, Phys. Part. Nucl. **28**, 134 (1997)
11. S.Kamerdzhiev, J. Speth, and G. Tertychny, Nucl. Phys. **A624**, 328 (1997)
12. S. Kamerdzhiev, J. Speth, G. Tertychny, and J. Wambach, Z. Phys. **A346**, 253 (1993)
13. G.R. Satchler and W.G. Love, Phys. Rep. **55**, 183 (1979)
14. H.L. Clark, Y.-W. Lui, and D.H. Youngblood, Nucl. Phys. **A589**, 416 (1995)
15. S. Kamerdzhiev, J. Speth, and G. Tertychny, Phys. Rev. Lett. **74**, 3943 (1995)
16. H. Diesener, U. Helm, G. Herbert et al., Phys. Rev. Lett. **72**, 1994 (1994)
17. H.L. Clark, Y.-W.Lui, D.H. Youngblood et al. Nucl.Phys. **A649**, 57c (1999)
18. S. Kamerdzhiev, J. Speth, G. Tertychny, and J. Wambach, Nucl. Phys. **A577**, 641 (1994)
19. S. Kamerdzhiev, J. Lisantti, P. von Neumann-Cosel et al. Phys. Rev. C **55**, 2101 (1997)